ORIGINAL ARTICLE

Objective computerised assessment of residual ridge resorption in the human maxilla and maxillary sinus pneumatisation

Ulrike Gerken[1] · Felix Esser[2] · Stephan C. Möhlhenrich[1,3] · Alexander K. Bartella[4] · Frank Hölzle[1] · Horst Fischer[2] · Stefan Raith[1,2] · Timm Steiner[1]

Abstract

Objectives Atrophic resorption of the maxillary alveolar ridge is a complication that makes implantological rehabilitation critical. Our aim was to develop a novel computer aided procedure for the accurate quantitative assessment of maxillary residual ridge resorption including pneumatisation of the maxillary sinus that goes beyond previously described approaches and to apply it to a large dataset.

Materials and methods To develop and refine the method, we performed a retrospective analysis using computed tomography data from 405 patients to generate segmented, three-dimensional models of zygomaticomaxillary bones and maxillary sinuses. Using anatomical landmarks and orientation lines or planes, all models were aligned automatically to subsequently generate cross-sectional images ($n = 2835$), enabling the classification of atrophy as well as the quantification of volumes and caudal extensions of the maxillary sinuses.

Results We developed and implemented an accurate and reproducible workflow for the semi-automated analysis of volumetric maxillary images. Comprehensive statistical analysis of the large quantitative dataset revealed various correlations of maxillary process heights and sinus volumes with atrophy class, age and region and identified conjectural trends over the patient group.

Conclusions The method was used successfully to process a large dataset to classify atrophy, to measure alveolar height parameters, and to quantify maxillary sinus volume, bottom volume and pneumatisation.

Clinical relevance Apart from the anthropometric value of the generated dataset, the method could be applied to provide additional and more accurate data to assess the necessity of bone augmentation in the context of three-dimensional planning before implantation.

Keywords Maxillary atrophy · Sinus pneumatisation · Maxillary sinus bottom volume · Three-dimensional analysing · Implantology · Sinus lift

Introduction

Over the last six decades, several authors have documented rapid, irreversible alveolar bone resorption and severe atrophy of the

maxillary alveolar ridge as a result of tooth loss [1–8]. As the jaw loses its tooth bearing function, the edentulous alveolar ridge suffers from chronic and constant bone loss due to reduced mechanical stimulation and the lack of physiological tensile strain [9, 10]. Disuse atrophy is therefore a continuous, cumulative procedure of bone osteolysis and remodelling, and it is described as progressive and irreversible [7, 9]. The average rate of vertical resorption of the anterior maxilla was found to be 0.1 mm (0–0.7 mm) per year varying among individuals and within individuals at different times [3, 10, 11] influenced by anatomic, biologic, psychosocial, metabolic, functional and prosthetic factors [3, 8–11]. Cawood and Howell postulate that alveolar ridge resorption follows a predictable pattern with initial horizontal bone loss and subsequent vertical resorption [4]. They claim that bone resorption will occur in the alveolar rather than the palatine process of the jaw. Furthermore, they point out that horizontal bone loss in the atrophying maxilla leads to a centripetal change in shape of the alveolar process, contrary to the primary centrifugal

Stefan Raith and Timm Steiner contributed equally to this work.

✉ Ulrike Gerken
ulli.gerken@gmail.com

1 Department of Oral and Maxillofacial Surgery, RWTH Aachen University Hospital, Pauwelsstraße 30, 62074 Aachen, Germany

2 Department of Dental Materials and Biomaterials Research, RWTH Aachen University Hospital, Pauwelsstraße 30, 52074 Aachen, Germany

3 Department of Orthodontics, University Witten/Herdecke, Alfred-Herrhausen-Straße 45, 58448 Witten, Germany

4 Department of Maxillofacial and Facial Plastic Surgery, University Leipzig, Liebigstraße 12, 04103 Leipzig, Germany

changes in the mandible, due to specific patterns of bone resorption and bone remodelling. Based on these findings, they subdivided the changes in shape of the alveolar processes into six now well-established classes [4].

Some literature claims that after tooth loss in the posterior maxilla, alveolar bone resorption occurs simultaneously with expanding maxillary sinuses, the so-called pneumatisation [12]. By this effect, the volume of the sinus increases. The sinking of the sinus to the region between residual teeth may also lead to maxillary sinus septa. Sinus septa are divided into those existing due to maxillary development and those arising due to irregular pneumatisation [13–15]. Nevertheless, Cawood and Howell's classification does not take pneumatisation into any account, and literature lacks a reliable method to obtain objective and quantitative measurements of maxillary bone reduction, and in particular pneumatisation effects. Haas et al. reviewed how computer-aided planning in orthognathic surgery is well established nowadays, but even though accurate data is requested in anthropometric research, as well as in orthodontics and maxillofacial surgery, we could not find reliable implementation in literature analysing atrophy and anthropometric maxillary data including maxillary sinuses [8, 16–19]. Only one very recent attempt could be found focusing on maxillary sinus depth, residual ridge height and sinus opening angle based on manually placed landmark points [20]. With the aim to improve the reproducibility of such three-dimensional image-based morphometric measurements, we have already conducted a study at our department by generating an objective computer-aided method to classify the atrophic changes of the mandible [21]. The study describes a method for the automated classification of bone resorption following Cawood and Howell's model using the three-dimensional medical imaging and tailor-made algorithm. The objective of the present work was to develop a simple and robust computer-assisted standardised method to reliably quantify a comprehensive set of maxillary anatomical features. We applied our method to a large set of maxillary CT (computed tomography) data and related the generated data to demographic parameters, such as age or gender, and classified levels of alveolar ridge resorption. For the first time, we provide data about the atrophic maxilla in combination with bottom volume of the maxillary sinus as additional descriptive value for pneumatisation, underlining the clinical value of our method, as it will help, e.g. optimising quantities of sinus lift grafts.

Material and methods

Patient data

We obtained 2387 CT scans of the head and neck region, all diagnostic images taken from the University Hospital Aachen's data pool between 2007 and 2015. The data pool has previously been used in anatomical studies for morphometric analysis of the mandible [21, 22], and all images have been acquired for clinical indications and not with the intention to generate data to be used in this study. Criteria for exclusion were bone fracture and history of facial trauma, bone transplant and augmentation, syndromes and dysostoses/congenital craniofacial anomalies, medication-related osteonecrosis of the jaw, osteoradionecrosis of the jaw, paranasal sinusitis or any maxilla or maxillary sinus tumour. Four hundred five datasets of primarily Caucasian patients (ethnicity was not protocolled) were selected and in accordance with the data protection directives we assigned each scan a randomised pseudonym and generated a dataset of three-dimensional images of healthy adult maxillary bones and sinuses. No consecutive scans of the same patients were included in the dataset.

Volumetric image acquisition and data segmentation

The CT scans were acquired using two different CT Scanners manufactured by Siemens Medical Systems (Erlangen, Germany), i.e. the Dual-Energy-CT SOMATOM Definition and the SOMATOM Definition AS, at a tube voltage of 120 kV. The slice thickness was kept between 0.5 and 1 mm to ensure sufficient quality. All imaging data were converted into DICOM (digital imaging and communication in medicine) file format and further processed using the software *Mimics* 14.0 (Materialise, Leuven, Belgium), a program that allows the creation of three-dimensional models based on volumetric medical imaging data. Skull models were built by selecting a bone mask with a threshold operation and subsequent region growing around the area of interest. To identify the maxillary bone surface, we used Hounsfield unit (HU) values with variable thresholds ranging from a minimum of 226 to a maximum of 3071, manually adapted to the individual apparent density of the bone. Due to the relatively low apparent bone density of the maxillary alveolar process, we completed the contour of the alveolar crest, tracing it by hand, only in those slices where the bone was not identified correctly based on threshold operations. Additionally, we created three-dimensional models of the maxillary sinuses by selecting the air-filled cavities again based on individually adapted thresholds (with HU values from − 1023 to − 250). Because of the generally low bone density of the maxilla, its individual variation in young and older patients of different gender and the occurrence of artefacts mainly caused by metal restorations and fixed prosthetic devices in some of the imaging data, the use of a constant threshold led to incomplete geometric features preventing proper data analysis. It was found that individually adjusting the threshold value range was less time-consuming than subsequent manual corrections. In order to separate the bony midface from the skull, a virtual Le-fort-III fracture was placed resulting in a zygomaticomaxillary segmentation, which includes the whole zygomatic arch, the

palatine and the nasal bone and a small part of the sphenoidale bone. This decision was taken, as it helped standardising the segmentation procedure based on clearly defined borders while the subsequent evaluation techniques ensured that only maxillary bone was investigated, and the surrounding bone parts had no biasing influence on any of the measurements. Therefore, to ensure that all virtual models were cut in a re-producible way at standardised locations, we defined the frontonasal and frontozygomatic sutures as delineation lines and cut distally from the zygomatic arch at the point where it joins and spreads into the squamous part of the temporal bone. The maxillary sinuses were segmented exploiting the air that is visualised inside these paranasal sockets and in its surround-ings (Fig. 1). Thus, being a result of both computerised and manual operations, we regard our procedure of image process-ing and segmentation as semi-automatic.

Anatomical landmarking and generation of cross-sections

Subsequent to the segmentation of upper jaws and maxil-lary sinuses, we exported the data in STL format (a standardised file format originally developed for additive manufacturing) to enable further data processing. Using Blender 2.75 (Blender Foundation, Amsterdam, The Netherlands), an open three-dimensional modelling and rendering suite, cross-section images were generated as described in the following. According Cawood and Howell [4], the alveolar and the basilar (palatine) processes are separated by a horizontal plane spanning through the two great palatine foramina (**GPF**) on the right and the left side as well as the incisive foramen (**IF**). Following our approach, we first localised these well-defined landmark points manually at each maxillary surface, to project this horizontal orientation plane using the closest point align-ment algorithm by Horn [23]. This plane, in the following called demarcation plane **d,** marked the demarcation be-tween the alveolar and palatine processes and at the same time was used to register all upper jaws in one common coordinate system to improve commensurability and as pre-condition for the following automated evaluation with al-gorithms. We defined additional landmarks and further ori-entation planes for each model, as illustrated in Figs. 2 and 3. With the curvature operation in Blender, we traced an alveolar crest line manually. Subsequently, an alveolar crest plane **c** was generated parallel to **d**. In contrast to the points **GPF** and **IF** and the plane **c**, which had to be assigned manually, a customised algorithm was programmed to au-tomatically identify the landmark points at the anterior na-sal spine (**ANS**) and posterior nasal spine (**PNS**) by detect-ing the maximum expansions of the segmented models in anterior and posterior direction, similar to a previously pub-lished algorithm detecting the pogonion at the mandible

[22]. A midsection plane (**ms**) was defined spanning through the previously placed landmarks **ANS** and **PNS** perpendicular to the demarcation plane **d**. Additional verti-cal cuttings perpendicular to plane **d** were placed automat-ically on each side of the upper jaw resulting in seven cross-sectional planes illustrated in Fig. 2b, c: referring to the midsection line as 0°, five cross-sections with angles of 0°, + 45°, − 45°, + 90° and − 90° were cut originating after one third of the midsection line between **ANS** and **PNS**, and another two cross-sections with angles of + 90° and − 90° were cut originating after two thirds of the midsection line between **ANS** and **PNS**, using customised algorithm similar to previously published work for the mandible [21]. All cross-sections (seven for each jaw) were assigned to four different regions based on their anatomical localisation. As shown in Fig. 2b, c, the right and left posterior cross-sections are located in the region of the second and third molar (region **m**), the right and left middle cross-sections (region **p**) in the region of the second premolar or some-times first molar, the right and left frontal cross-sections (region **ca**) in the region of the canines or first premolars, while the midsection (region **i**) matches the midsection plane. Within all cross-sections, a point **D** was automatical-ly generated at the height of the demarcation plane **d** by a vertical projection through the alveolar crest starting at point **C** (Fig. 3). Point **B** as shown in Fig. 3 represents the lowest expansion of the maxillary sinus within each of the posterior cross-sections **m** and **p.**

Atrophy classification

We applied the classification introduced by Cawood and Howell (Fig. 4, upper left panel) to categorise all cross-sections ($n = 2835$) of the upper jaws with respect to atrophy by visual judgement. To improve accuracy, one examiner per-formed the classification at three consecutive time points. In cases where cross-sections were ambiguously sorted into two adjacent classes the class chosen twice was assigned to the respective cross-section. Figure 4 (lower panels) illustrates schematically how two-dimensional cross-section images are assigned to one of the six atrophy classes. Once all the seg-ments had been classified, automated geometrical height mea-surements were conducted.

Determination of alveolar ridge heights and maxillary sinus volume

Two-dimensional measurement in every cross-section deter-mined maxillary ridge heights and pneumatisation effects. Therefore, the following vertical distances of the maxillary ridge were measured as shown in Fig. 3:

Fig. 1 Segmentation of CT slices and three-dimensional volume reconstruction. Screenshots of different CT slices with segmentation of the maxilla and maxillary sinuses processed with a region-growing method (**a** coronal, **b** transverse and **c** sagittal); and three-dimensional volume reconstruction of maxilla and maxillary sinuses (**d** front, **e** back and **f** basal) as visualized by the Mimics software
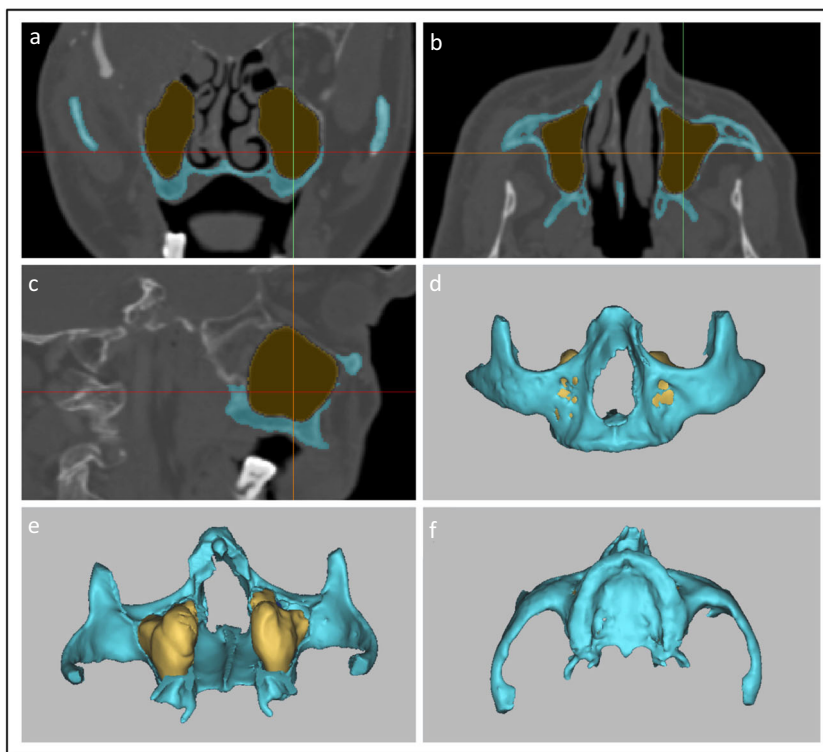

Fig. 2 Illustration of landmarks and cross-sections. Panel **a** shows the location of the following landmarks (red font): anterior nasal spine (ANS) and posterior nasal spine (PNS) interconnected by the midsection line (ANS to PNS, shown in green), right and left great palatine foramina (GPF) and incisive foramen (IF). Panel **b** shows the placement of seven cross-sections (dark-blue lines) for each maxilla assigned to four different region-dependent groups (light blue font). (m) region of the second and third molar; (p) region of the second premolar/first molar; (c) region of the canine/first premolar; (i) midsection. The three-dimensional location of the landmarks and cross sections is shown in panel **c** showing a bottom view of a reconstructed dentate maxilla
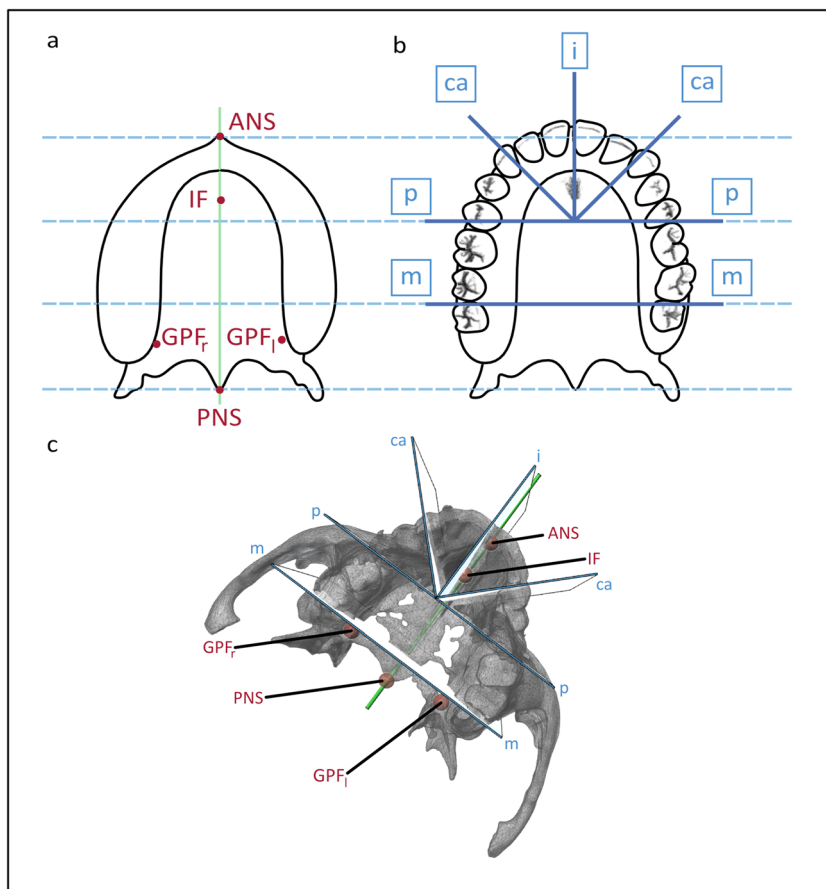
(1) **C–D** alveolar crest to demarcation plane (alveolar process height)
(2) **C–B** alveolar crest to bottom of the maxillary sinus (residual ridge height)
(3) **D–B** bottom of the maxillary sinus to demarcation line (maxillary sinus depth)

Additionally, we employed an algorithm to calculate the total volumes of the maxillary sinuses (left and right sinus volumes were calculated individually). We also calculated the maxillary sinus bottom volume as quantitative parameter of pneumatisation by projecting a horizontal plane (**pn**) parallel to plane **d** 12 mm above the point **C** (at regions **m** and **p**), using it to calculate the maxillary sinus volume underneath it. The distance of 12 mm was chosen because 12 mm of bone supply can be considered as optimal bone supply for stable implants.

Statistical analysis

To enable proper interpretation of the results, we performed statistical evaluation of the following correlations:

a) Atrophy classes and regions in relation to age
b) Alveolar ridge height distances (**C–D**, **C–B**, **D–B**) in relation to atrophy class
c) Residual ridge height (**C–B**) in relation to maxillary sinus depth (**D–B**)
d) Maxillary sinus bottom volume in relation to atrophy class
e) Maxillary sinus volumes in relation to atrophy class, gender and age

Results were analysed using the Prism 8 data visualisation and analysis suite (GraphPad Software, San Diego, Ca, USA). For correlation analysis ($p < 0.05$, two-tailed), we calculated Pearson's correlation coefficients for normal distribution, and Spearman's correlation coefficients for non-normal distribution data. For correlation analysis that included the classifications of atrophy, the class numbers were considered as ordinate values.

Results

Method workflow

In the context of this work, we have established a well-defined, semi-automated workflow that enables the accurate determination of CT scan–derived volumetric images to classify and quantify maxillary ridge resorption (atrophy) along with maxillary sinus volume and volume of pneumatisation. The workflow (shown in Fig. 5)
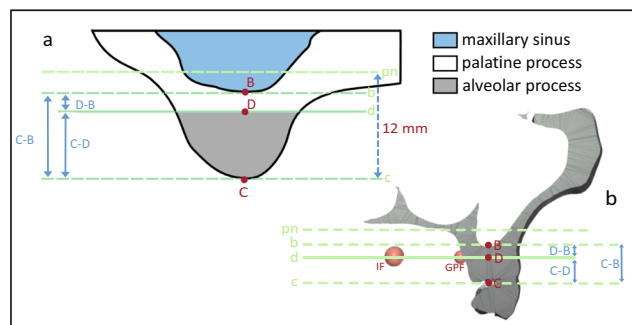

Fig. 3 Illustration of alveolar and palatine process dimensions. Panel **a** illustrates the location of orientation planes b, c, d and pn (indicated in green, lower character, lines shown in green) and corresponding measuring points (indicated in red, upper character). Measured distances are indicated in blue arrows. Anatomical regions in the cross-section are indicated with the following colours: maxillary sinus blue, palatine process white and alveolar process grey. Panel **b** illustrates the location of planes, points and distances using a cross-section of region p derived from a reconstructed 3-D-model. Landmark points GPF and IF are shown as red spheres

includes the selection of CT data, the building of raw three-dimensional models to enable segmentation, followed by the introduction of anatomical landmarks (**ANS, PNS, IF, GPF, B, C** and **D**) as well as orientation lines

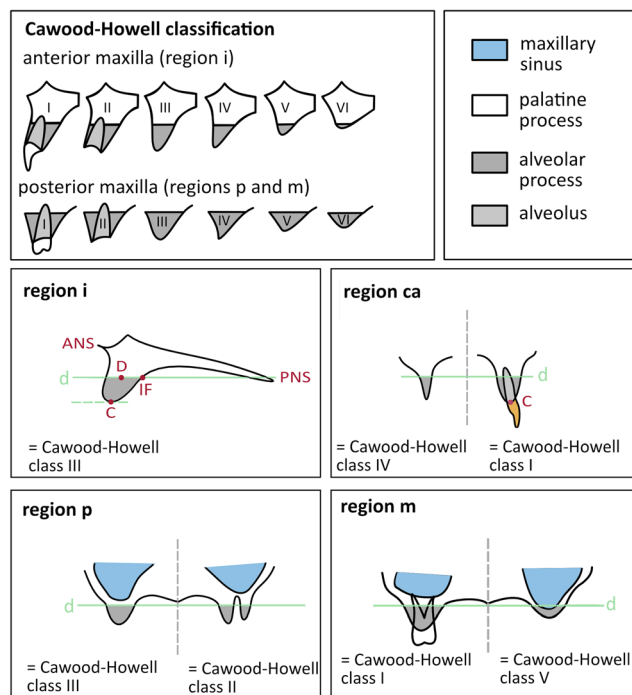**Fig. 4** Cawood and Howell classification and anatomic dental chartings of cross-section regions m, p, ca and i. Upper panel shows the atrophy classes I–VI, both for the anterior maxilla (midsection region i) and the posterior maxilla (cross-section of anatomical regions m and p), in an illustration adapted from Cawood and Howell, 1988. Anatomical regions in the cross-section indicated with the following colours: maxillary sinus blue, palatine process white, alveolar process grey and alveolus light grey. Lower panels show details regarding the different cross-section regions m, p, ca and i, including relevant measuring and landmark points (indicated in red, upper character) as well as planes indicated in green

and planes (**b**, **c**, **d**, **ms** and **pn**) to allow for the generation of cross-sections as a basis for classifying and calculating maxillary parameters to, finally, perform statistical analysis. Automated operations were used for file conversion steps, during the generation of raw three-dimensional models, as well as for the projection of orientation planes and the definition of some anatomical landmark points.

Data analysis

The study group compromised 405 patients aged 18 to 97 with a mean age of 59.66 years. Figure 6 a illustrates the age distribution of the patient collective. 247 (61%) were male and 158 (39%) were female. 47% of all cross-sections ($n = 2835$) were dentate and 53% were edentulous.

Atrophy classes and regions in relation to age

In the investigated dataset, only 14 cross-sections were assigned to Cawood-and-Howell-class II (empty alveolar cavity). Because of the relatively short period between tooth extraction and bone healing, this low number is very plausible but being too small for statistically sound evaluations (0.5%), this group was excluded from the datasets used for statistical evaluation. In marked contrast to classes IV ($n = 128$; 5%) and VI ($n = 118$; 4%), a larger number of cross-sections were assigned to Cawood-and-Howell-class III ($n = 543$; 19%) and V ($n = 698$; 25%). Cross-sections were assigned to their corresponding regions **m**, **p**, **ca** and **i**, (refer to Fig. 2b, c). Regions **ca** and **i** contained more dentate (class I) cross-sections (59% and 54% respectively), compared to regions **p** and **m** (35% and 43% respectively), which were composed of more edentulous (classes II–VI) cross-sections (Fig. 7). As shown in Fig. 6b, age medians for all cross-section regions **m**, **p**, **ca** and **i** increase generally from class I to VI. The only exception is class V that shows a younger mean age as class IV in all four regions. Correlation analysis was performed revealing a weak but yet significant (P values < 0.0001 for all classes) positive correlation of class value (I–IV) and age for all regions (Spearman's r values: **m** = 0.3831; **p** = 0.4772; **ca** = 0.4786; and **i** = 0.4355).

Alveolar ridge height distances in relation to atrophy class

To investigate possible trends, changes in vertical heights (i.e. distances **C–D**, **C–B** and **D–B**) were analysed in relation to atrophy classes as illustrated in Fig. 8 showing the following results.

(1) Distance **C–D** (alveolar crest to demarcation plane) is the vertical height of the alveolar process and varies between 2.2 and 18.8 mm in the posterior maxilla and between 0.1 and 14.8 mm in the anterior maxilla. Alveolar process height **C–D** is negatively correlated to class value.

As shown in Fig. 8a, distance **C–D** generally decreases significantly with higher classes in all regions (Pearson/Spearman r values: **m** = − 0.4348; **p** = − 0.5688; **ca** = − 0.6173; and **I** = − 0.5666), and this trend is more pronounced in the frontal regions **ca** and **i** than in the two posterior regions **m** and **p**. As illustrated, dentate ridges (i.e. class I) reveal the highest values and show a large spread of values in the frontal regions **ca** and **i**. Class I medians of regions **m**, **p**, **ca** and **i**, are 12.6 mm, 11.7 mm, 8.1 mm and 6.7 mm respectively.

(2) Distance **C–B** (alveolar crest to bottom of maxillary sinus) describes the total residual ridge height between the alveolar crest and the lowest point of the sinus maxillaries, which serves as the vertical bone supply of the posterior maxillary regions. As shown in Fig. 8b, we observed residual ridge heights between 1.2 and 38.9 mm. Similar to the alveolar process height, the residual ridge height **C–B** generally decreases significantly with higher classes in all regions (Spearman r values: **m** = − 0.7084; **p** = 0.5827;). In the regions **m** and **p**, class III medians are 11 mm and 12.8 mm respectively, class V medians are smaller with 6.5 mm and 6.1 mm, and class VI medians decrease further to 2.6 mm and 2.8 mm. As shown in Fig. 8a, b, in class III cross-sections of regions **m** and **p**, the median distance **C–B** is slightly greater than the median distance **C–D**, which implies that point **B** lies in the palatine process slightly above the demarcation plane **d**. Differently, in the progressed atrophy classes V and VI, the median of distance **C–B** is smaller than the distance **C–D**, meaning that here, point **B** is located in the alveolar process below **D** indicating a higher degree of pneumatisation in these classes.

(3) Distance **D–B** (demarcation to bottom of maxillary sinus) refers to the sinus depth. In region **m** and **p**, positive median values for class III and VI and negative values for class V and VI are shown. Since point **D** is fixed, positive values mean that **B** lies above **D** and negative values mean **B** is located below **D** (Fig. 8c). As for the previously analysed maxillary ridge descriptors **C–D** and **C–B**, we determined a negative correlation between distance **D–B** and class value for the two regions **m** and **p** (Pearson/Spearman r values: **m** = − 0.3455; **p** = − 0.3071).

Residual ridge height (C–B) in relation to maxillary sinus depth (D–B)

Figure 9 shows significant positive correlations between sinus depth and residual ridge height in both regions **m** and **p** (Pearson/Spearman r values: **m** = 0.6874, **p** = 0.4592). Therefore, decreasing bone supply (**D–B**) is associated with a sinking of the maxillary sinus bottom **B**.

Fig. 5 Method workflow overview. Illustration of the subsequent steps of our semi-automated method from the initial data pool towards a comprehensive set of quantitative data ready for statistical analysis. Important intermediate results or classification and calculation operations are shown in white boxes, while the connecting process steps are described in white font on blue arrows
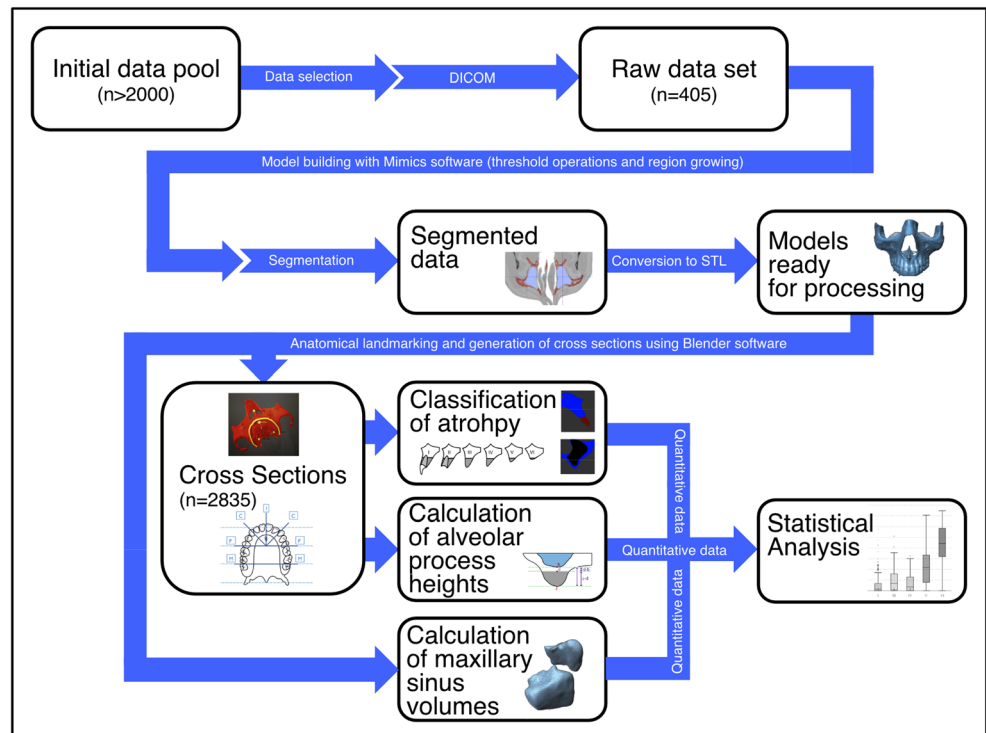
Maxillary sinus bottom volume in relation to atrophy class

Figure 10 shows the calculated volumes of the bottom part of the maxillary sinuses under a horizontal plane (**pn**) that was drawn 12 mm above point **C** at regions **m** and **p** plotted against classes I to VI. For both regions, median volumes referring to classes I, III and IV are below 0.5 cm^3 and increase with atrophy classes V and VI with a median of 1.26 cm^3 (class V) and 2.47 cm^3 (class VI) for region **p** and of 0.95 cm^3 (class V) and 2.2 cm^3 (class VI) for region **m** respectively. Overall, we see a significant positive correlation of the maxillary sinus bottom volume with higher classes (Spearman r values: **m** $= 0.6642$, **p** $= 0.6528$).

Maxillary sinus volumes in relation to atrophy class, gender and age

Complete maxillary sinus volumes of all available 653 sinuses range from 3.03 to 34.18 cm^3. Their mean volume is 16.31 cm^3 with a standard deviation of 5.47 cm^3 (Table 1). The table shows results as mean values for better comparison with results from literature, and median values in brackets. Comparing gender, volumes are larger in males than females; comparing age groups, volumes are larger in young people than old people; regarding atrophy classes, volumes are highest in patients with dentition (class I) and in patients with severe atrophy (class VI).

Discussion

Method

In this study, we present a semi-automated method workflow to gather a set of relevant anatomical data related to alveolar residual ridge resorption and alveolar sinus pneumatisation of the upper jaw. Accurate and reproducible acquisition of such data can be regarded as an important prerequisite for both advanced anthropometric studies and three-dimensional assisted planning of implantation and sinus floor augmentation. The proposed set of landmarks, reference lines and orientation planes will ensure a maximal degree of comparability between totally different or consecutive datasets obtained in the context of follow-up studies. Due to the large number of patients distributed over a wide age range, our anatomical data show statistically significant trends that align well with previously published data from studies based on fully manual evaluation, confirming the reliability of our semi-automated approach. Even though we successfully used the method to confirm atrophy-induced pneumatisation for the first time, we see some room for further improvements in the future. In the context of this study, it was not possible to automate all required operations and some manual steps remain. The first manual step in our method is the individual adaptation of threshold values to enable the proper identification of the maxillary bone surface as well as the borders of the maxillary sinuses by automated threshold
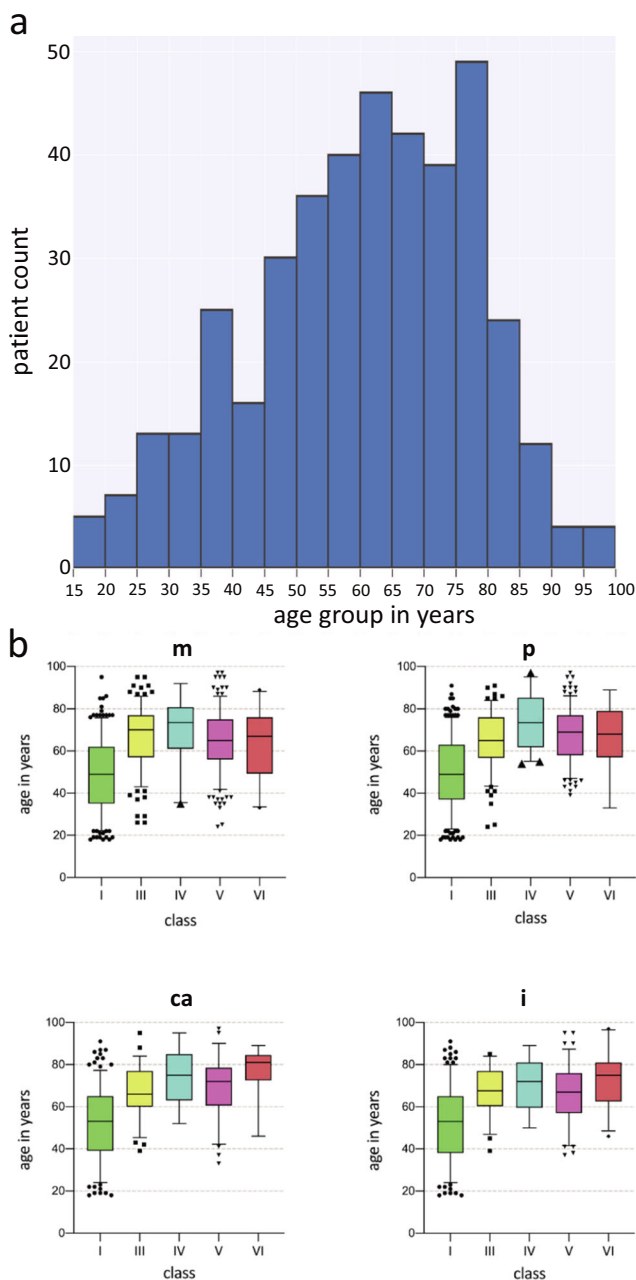
Fig. 7 Region dependent distribution of atrophy classes. Pie charts illustrating the proportional occurrence of Cawood and Howell's atrophy classes in the different regions (m, p, ca and i)

Fig. 6 Age distribution of patient collective and in relation to atrophy classes. Panel **a** shows the age distribution of the patient collective. Age groups were defined using 5-year intervals and plotted as blue bars against patient number per group. Panel **b** illustrates the age distribution in relation to atrophy classes by region (m, p, ca and i). Coloured boxes represent the interquartile range. Whiskers indicate the 95th and 5th% quartiles. Data points outside the 5–95% range are shown as solid black dots. Black lines indicate medians. The following colours have been assigned to atrophy classes: I, green; III, yellow; IV, cyan; V, pink; VI, dark red; and are being used for these classes in all subsequent illustrations
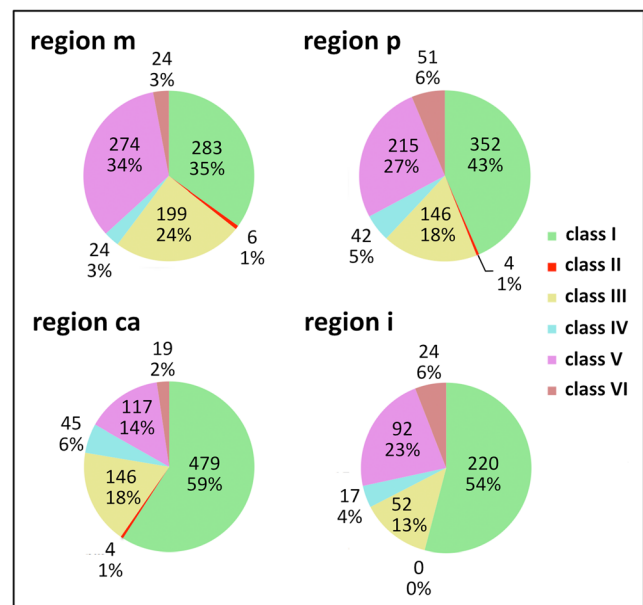
operations. Still, in some cases, the contour of the alveolar crest had to be traced manually. In a similar study on mandibular atrophy classification performed in our department by Varga et al., a fixed threshold range could be used throughout a large dataset [21]. The need for individual adaptation of threshold values in this study results from the more variable and generally lower bone density found in the upper jaw compared to the more uniform situation in the lower jaw [24]. Customised normalisation or compression algorithms could be developed to avoid manual adjustment of threshold values and contour tracing to improve the reproducibility and at the same time reduce the workload particularly during work with larger sets. The localisation of three landmarks GPF, IF and C was performed manually. Therefore, the development of algorithms that automatically detect these landmarks would further improve the degree of automation. Another target for future optimisations is the classification of maxillary alveolar atrophy. As mentioned earlier, the automatic determination of mandibular atrophy classes by Varga et al. demonstrated a high degree of accordance between human examiners and the used algorithm [21]. Based on these promising results, a corresponding strategy could be developed for the maxillary region. The use of CT scans instead of cone beam computed tomography (CBCT) could be regarded as another limitation of this study. We chose to use CT scans (the gold standard in orofacial imaging for the last decades) mainly because large retrospective
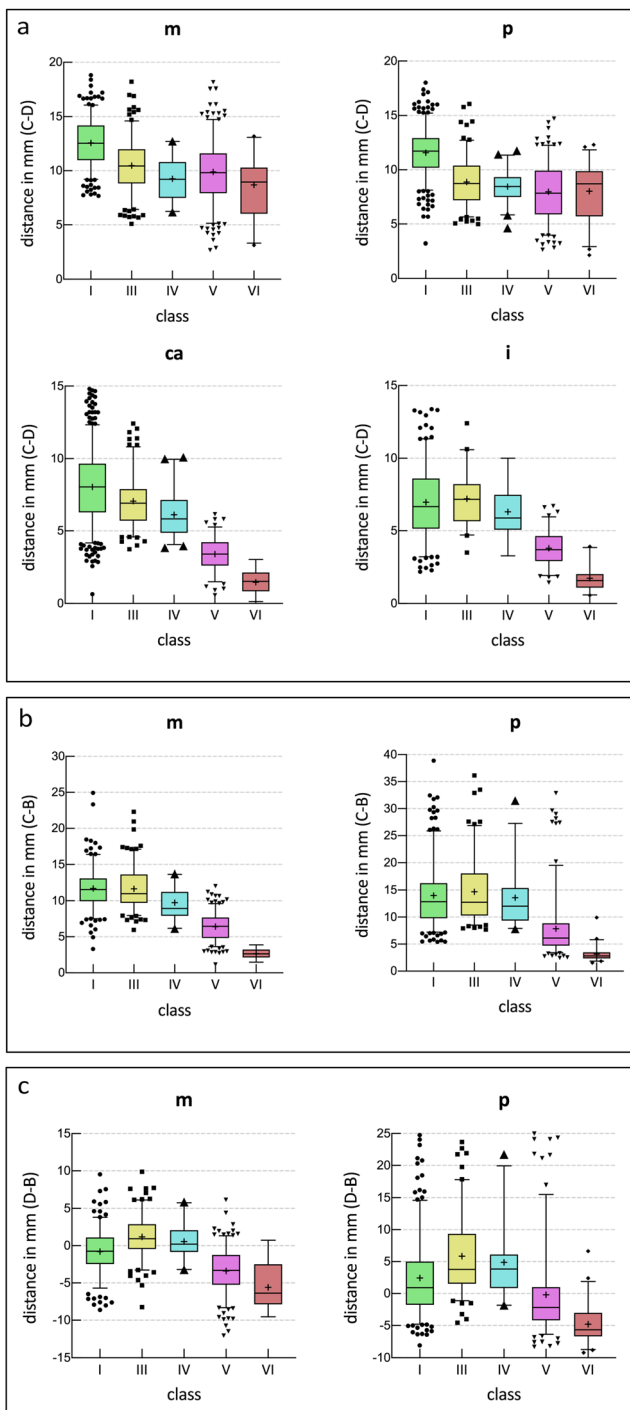
Fig. 8 Vertical heights C–D, C–B and D–B correlated to classes I–VI in the different regions. Panel **a** shows the distance C–D (alveolar process height) in the regions m, p, ca, and i. Panel **b** shows the distance C–B (total residual ridge height) in the regions m and p. Panel **c** shows the distance D–B (sinus depth) in the regions m and p. In all panels, coloured boxes represent the interquartile range. Whiskers indicate the 95th and 5th% quartiles. Data points outside the 5–95% range are shown as solid black dots. Black lines indicate medians; mean values are indicated by black cross symbols

datasets were readily available. Anyhow, acknowledging the increasing use of CBCT instead of CT, it would be helpful to include CBCT image processing in the workflow to reduce radiation exposure. Finally, it should be noted that a publicly available freeware like InVesalius 3 (provided by Tridimensional Technology Division—Center for Information Technology Renato Archer [25]) could be applied to perform image processing operations instead of the proprietary software Mimics used in this study.

Data analysis

Atrophy classification

A report from the 4th International Congress on Preprosthetic Surgery, in 1991, suggests that Cawood and Howell's research on the stage of alveolar ridge resorption delivered the best professionally qualified classification system up to that time [26]. To date, this classification is still of value; however, it simplifies the issue, as already criticised by Eufinger et al. [6]. Atrophy is not yet fully understood due to the multiplicity of factors affecting the rate of changes in the external shape and internal structure of the alveolar ridge. The consistent reported finding that atrophy increases with age, correlating with prolonged edentulism [8], is in accordance with our results, while we cannot underscore the distinct patterns of atrophy stages that the classification assumes, i.e. in our study, the edentulous cross-sections classes III and V occur in large numbers, whereas class IV and VI were only sparsely observed in the data pool of this study. Regarding class IV, the jaw's transformation time in a knife-edged state might be either extremely short and, thus, underrepresented in the data, or it might not be a distinct state during the process of atrophy as it has been suggested until now. Further investigation is needed, as literature lacks evidence. The small amount of class VI's cross-sections implies that severe atrophy is not an expected progression, but rather seldom and a pathological condition. In our study group, the anterior upper jaws comprise more dentate cross-sections than the posterior jaw regions, which reveal that tooth loss occurs earlier in multi-rooted regions than in the single rooted frontal regions.

Maxillary bone height and pneumatisation influence

Alveolar ridge reduction impacts on all ageing individuals and must be thoroughly understood by dentists, as well as oral and maxillofacial surgeons. Due to the projected demographic change, i.e. the increasing number of elderly people, clinical survey data reinforces that there will be an increased need for treatment of the edentulous jaw. Aesthetics, comfort, stability

and ability to talk and chew are factors that influence one's quality of life and there is a pronounced demand for functionally adequate prosthetic replacement of lost teeth nowadays [27, 28]. Moreover, patients with implant over-dentures are more satisfied than those with full dentures [29]. In the following, maxillary atrophy and pneumatisation patterns in the posterior maxilla based on the cross-sectional analysis of our available population are discussed. As expected, the greatest alveolar process height (measured as distance **C**–**D**) is found in dentate ridges (class I). At the same time, the large number of reduced dentate ridges due to untreated periodontitis, i.e. not yet lost or extracted teeth held by an ill periodontal apparatus, which occurs especially in the anterior maxilla, provides a basis for the assumption that people hesitate and prefer to avoid anterior tooth extraction more than posterior tooth extraction [30]. In our study, a distinct pattern of alveolar part atrophy is especially shown in the frontal regions, represented by the cross-sections of regions **ca** and **i** as the distance **C**–**D** significantly decreases with higher classes. In distal regions, though, the decrease of distance **C**–**D** for classes III to VI as the alveolar crest point **C** moves in cranial direction is shown less distinctly. Instead, additional reduction from the cranial direction, resulting from the sinking of the sinus bottom, leads to reduced ridges. These findings strongly indicate that atrophy is taking place in the palatal process in the posterior regions due to pneumatisation and disproves Cawood and Howell's postulation that resorption only takes place in the alveolar part of the jaw. The distance **C**–**B** defines the total vertical bone height in the posterior maxilla and is especially relevant for planning the insertion of dental implants. If bone height is not adequate, bone augmentation will be necessary to ensure successful implantation. Measured median (and mean ± SD) bone heights of class III ridges are 11 mm (11.7 ± 2.7 mm) in the region of the second molar, and 12.8 mm (14.7 ± 5.8 mm) in the region of the second premolar/first molar and indicate sufficient vertical bone supply for successful implantation. It is to keep in mind, that the distance **C**–**B** does not describe the exact axis of implant insertion, while angled insertion requires less supply of vertical bone height and more of bone width, indicating that additional 3-D data should be used to support such procedures. Caused by atrophy through ridge reduction and pneumatisation total maxillary ridge heights in classes V (medians 6.5/ 6.1 mm) and VI (medians 2.6/ 2.8 mm) appear insufficient for insertion of most regular implants. The distance between **D** and **B** provides evidence for pneumatisation and illustrates its dimension. Based on positive values for classes I, II and III at rather young ages, we conclude that in young healthy individuals, the bottom of the maxillary sinus (**B**) usually lies above **D** in the palatal process. As atrophy progresses, the sinus floor sinks, according to the decrease of distance **D**–**B**. Negative values occur as the sinus floor sinks under the plane **d** into the alveolar process. Values continue to decrease with higher
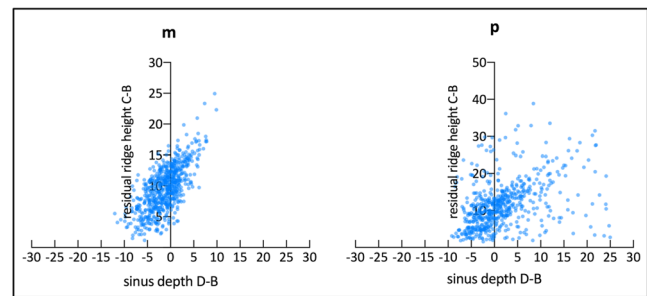

Fig. 9 Correlation between residual ridge height C–B and sinus depth B–D for regions m and p
Data points are shown as translucent blue dots

atrophy classes, which are primarily found in elderly patients. Like Wagner et al. [20], in our study, we observed a positive correlation of sinus depth and alveolar height. Anyhow, in contrast to our findings, they conclude that sinus depth is independent of age and dentition, a constitutional trait and a stable variable. This contradicts the concept of atrophy-induced pneumatisation. With a similar conclusion, another retrospective study conducted by Schriber et al. [31] did not reveal a significant correlation between sinus dimensions (as measure of pneumatisation) and dentate or edentulous state of the posterior maxilla. Based on the dataset acquired in our study, though, we clearly show that sinus depth and alveolar bone height are influenced by pneumatisation in the course of atrophy. We believe that the main reason why Wagner et al. and also Schriber et al. could not observe pneumatisation effects in their study is the comparatively rough separation of sinus dimensions data into a dented and an edentulous group. In our approach, we classified the cross-sections according to Cawood and Howell's classes to enable a more differentiated analysis of the pneumatisation process. As shown in Fig. 8c, the sinus height means and medians are in the same range for classes I–IV before decreasing rapidly in classes V and VI. It becomes clear that pneumatisation effects are mainly restricted to these higher edentulous atrophy classes V and VI. By grouping all edentulous atrophy classes (II–VI) into one
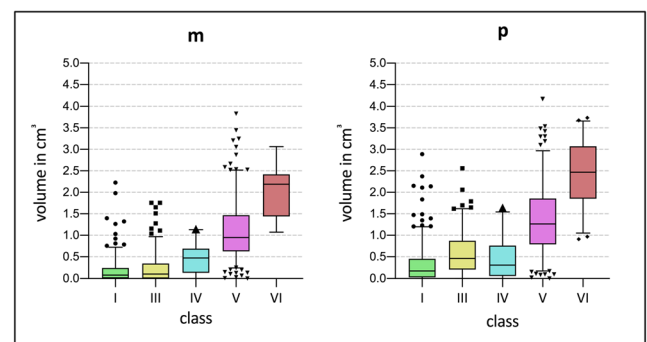

Fig. 10 Bottom volumes of the maxillary sinuses (cm³) correlated to classes I–VI for regions m and p. Coloured boxes represent the interquartile range. Whiskers indicate the 95th and 5th% quartiles. Data points outside the 5–95% range are shown as solid black dots. Black lines indicate medians

Table 1 Maxillary sinus volumes (cm^3)

TOTAL (n = 653)	Mean ± SD	Median
All	16.31 ± 5.47	16.07
GENDER		
Men	17.58 ± 5.75	17.24
Women	14.43 ± 4.42	14.43
AGE		
18 – 45	18.13 ± 5.87	18.71
46 – 100	16.05 ± 5.40	15.73
CLASSIFICATION (in region p)		
Class I	17.39 ± 5.33	17.10
Class III	13.82 ± 4.60	13.66
Class IV	13,01 ± 4.44	12.69
Class V	16.42 ± 5.29	16.10
Class VI	19.66 ± 5.34	19.54

group, the effect of pneumatisation may not be observed especially when more samples are assigned to the atrophy classes II–IV, in comparison to V and VI, which occur predominantly in older patients. Furthermore, the data acquired for the dentate groups could contain cross-sections with ill or dead teeth remaining in the jaw while lost bone function and periodontitis had led to residual ridge loss and pneumatisation in those dentate regions. These cases could lead to low values measured in the corresponding cross-sections and thereby prevent the proper identification of pneumatisation. By analysing the data grouped in atrophy classes, we prevented this effect and possible influences of the age distribution. Anyhow, further studies with consecutive CBCT data (once a corresponding workflow has been implemented) that is gained periodically from the same and patients over a lifelong period would be required to provide further insight into pneumatisation processes. Additionally, we assume a higher comparability of our data due to our workflow. While in the aforementioned study, sinus depth was measured in relation to the palatal plate identified by two reference points that need to be defined newly in every cross-section, we referred it to the previously described [4] demarcation plane **d**, which has the advantage that it is a well-defined three-dimensional anatomical reference plane that can be used to reliably register all models before analysis.

Maxillary sinus bottom volumes

As discussed above, our findings on positive correlations of maxillary bottom volumes with higher classes give basis to assume that in the progress of later atrophy stages (classes V and VI) the alveolar ridge reduction in the posterior maxilla occurs from cranial direction with the bottom of the sinus sinking (**B** sinks towards and below the point **D**), rather than from alveolar direction (the distance of the alveolar crest **C** to

the anatomical defined fixed point **D** is not decreasing much from atrophy class III to VI). Generally speaking, this assumes that sinus lifting should be the preferred augmentation procedure prior to implantation; however, only individual analysis will detect whether sinus grafting or vertical augmentation procedure, or a combination of both, have priority in preprosthetic surgery of the distal maxilla. Furthermore, with our method to gain data on the bottom volume of the maxillary sinuses, we can provide valuable information to predict the amount of sinus lift bone substitutes, i.e. the values for the sinus bottom volumes shown in Fig. 10 correspond to the quantity of bone substitutes needed for sinus elevation resulting in a total ridge height of 12 mm, in cases where no additional onlay reconstruction of the alveolar ridge is needed.

Maxillary sinus volumes

During the past decade, a few attempts were made to automatically measure maxillary volume on computed tomography data, and to analyse critical factors for volumetric changes. Cho et al. have already shown that age and alveolar bone height both have negative impact on maxillary sinus volume [32]. They report a mean volume of 20.78 cm^3, being noticeable higher than our results of 16.31 cm^3. This is most likely the result of a reduced age range on their side, as well as younger mean age (32.7 years compared to 59.7 in this study) and a smaller sample group of only 52 subjects. In a CT-based study on sinus dimensions Sahlstrand–Johnson et al. reported, that maxillary volumes are significantly lower in female compared to male subjects and simultaneously, they did not find a statistically significant correlation with age [33]. When comparing this result to ours, it has to be taken into account that their study is also based on a smaller patient group (60) with a mean age of 40 and a smaller age range of 18 to 65. The study of Möhlhenrich et al. recently described how gender and dentition (fully dentate, partly dentate and edentulous) correlate with the volume and surface of the maxillary sinus [34]. In accordance with their work, we observe that on average females have smaller sinuses compared with men. They could observed significant correlations of sinus volumes with certain tooth statuses but could not show a general correlation between volume and tooth loss (from fully dentate jaws to partly and finally fully edentulous), presumably because age was not taken into account in the context of this study; although, a negative correlation between age and maxillary sinus volume has been previously reported [32]. To take a differentiated, statistically solid look at maxillary sinus volumes in our study, we have investigated a large patient group (653 maxillary sinuses from 354 patients) with a higher mean (59.7) and a wide spread of age (18–97) to also cover higher atrophy classes mainly occurring in elderly patients over 60. In contrast to previous comparable studies, our data very clearly shows that maxillary sinus volumes are negatively correlated with age

finding the largest volumes in young and fully dentate patients and the smallest volumes in older patients when looking at the total sample population, whereas at the same time older patients who suffer from severe atrophy (class VI) show the largest volumes. Therefore, and for the first time, we reliably show that maxillary sinus volume on the one hand generally decreases with age, but on the other hand increases with severe alveolar bone loss due to pneumatisation effects mostly in elderly patients. Because of these adverse trends, correlation between age and volume should be analysed within same dentition or atrophy classes and correlation between class and volume should be analysed among the same age groups of sufficient sample size, to provide the most meaningful data. The importance of this is underlined by the results of Schriber et al. who did not observe a correlation between sinus dimensions and dentition, most probably because of their relatively low sample size in combination with an unbalanced age distribution of both the dentate and the non-differentiated edentulous group.

Conclusion

In this study, we developed a reproducible method enabling the semi-automated, computer-aided measurement of maxillary bone using three-dimensional imaging data to investigate alveolar atrophy. Applying our semi-automated workflow featuring the generation of maxillary region-specific cross-sections based on well-defined landmarks to a large patient pool that covers a wide age range and all stages of atrophy, we generated a comprehensive set of anthropometric anatomical data of the human maxilla and maxillary sinuses. Based on this data, it was possible to confirm atrophy-induced pneumatisation and quantify its dimension and the values of the actual bone supply measured by the vertical height, from the alveolar crest to the bottom of the sinus. In contrast to other studies that have used smaller and younger patient groups, our data convincingly shows that besides alveolar ridge resorption, the pneumatisation of alveolar sinuses is an important part of the alveolar atrophy process. The strong positive correlation between the degree of pneumatisation and atrophy class has clinical relevance, since it indicates that early implantation should be recommended to prevent complications resulting from insufficient bone supply caused from advanced pneumatisation. Because the precision and reproducibility of the method, similar individualised measurement could be included in standard three-dimensional planning before implantation with augmentation. Therefore, our study is especially of value from the anthropometric and implantological point of view.

Compliance with ethical standards

Conflict of interest The authors declare that they have no conflict of interest.

Ethical approval This article does not contain any studies with human participants or animals performed by any of the authors.

Informed consent For this type of study, formal consent is not required.

References

1. Atwood DA, Coy WA (1971) Clinical, cephalometric, and densitometric study of reduction of residual ridges. J Prosthet Dent 26(3): 280–295
2. Atwood DA (1963) Postextraction changes in the adult mandible as illustrated by microradiographs of midsagittal sections and serial cephalometric roentgenograms. J Prosthet Dent 13(5):810–824. https://doi.org/10.1016/0022-3913(63)90225-7
3. Tallgren A (1972) The continuing reduction of the residual alveolar ridges in complete denture wearers: a mixed-longitudinal study covering 25 years. J Prosthet Dent 27(2):120–132
4. Cawood JI, Howell RA (1988) A classification of the edentulous jaws. Int J Oral Maxillofac Surg 17(4):232–236
5. Cawood JI, Howell RA (1991) Reconstructive preprosthetic surgery. I. Anatomical considerations. Int J Oral Maxillofac Surg 20(2):75–82. https://doi.org/10.1016/S0901-5027(05)80711-8
6. Eufinger H, Gellrich NC, Sandmann D, Dieckmann J (1997) Descriptive and metric classification of jaw atrophy. An evaluation of 104 mandibles and 96 maxillae of dried skulls. Int J Oral Maxillofac Surg 26(1):23–28
7. Atwood DA (1971) Reduction of residual ridges: a major oral disease entity. J Prosthet Dent 26(3):266–279
8. Reich KM, Huber CD, Lippnig WR, Ulm C, Watzek G, Tangl S (2011) Atrophy of the residual alveolar ridge following tooth loss in an historical population. Oral Dis 17(1):33–44. https://doi.org/10.1111/j.1601-0825.2010.01699.x
9. Bodic F, Hamel L, Lerouxel E, Basle MF, Chappard D (2005) Bone loss and teeth. Joint Bone Spine 72(3):215–221. https://doi.org/10.1016/j.jbspin.2004.03.007
10. Atwood DA (2001) Some clinical factors related to rate of resorption of residual ridges. J Prosthet Dent 86(2):119–125. https://doi.org/10.1067/mpr.2001.117609
11. Carlsson GE (2004) Responses of jawbone to pressure. Gerodontology 21(2):65–70
12. Ulm CW, Solar P, Krennmair G, Matejka M, Watzek G (1995) Incidence and suggested surgical management of septa in sinus-lift procedures. Int J Oral Maxillofac Implants 10(4):462–465
13. Beretta M, Cicciu M, Bramanti E, Maiorana C (2012) Schneider membrane elevation in presence of sinus septa: anatomic features and surgical management. Int J Dent 2012:261905. https://doi.org/10.1155/2012/261905
14. Pommer B, Ulm C, Lorenzoni M, Palmer R, Watzek G, Zechner W (2012) Prevalence, location and morphology of maxillary sinus septa: systematic review and meta-analysis. J Clin Periodontol 39(8):769–773. https://doi.org/10.1111/j.1600-051X.2012.01897.x
15. Underwood AS (1910) An inquiry into the anatomy and pathology of the maxillary sinus. J Anat Physiol 44(Pt 4):354–369

16. Haas OL Jr, Becker OE, de Oliveira RB (2015) Computer-aided planning in orthognathic surgery -systematic review. Int J Oral Maxillofac Surg 44(3):329–342. https://doi.org/10.1016/j.ijom.2014.10.025

17. Kasai N, Kondo O, Suzuki K, Aoki Y, Ishii N, Goto M (2018) Quantitative evaluation of maxillary bone deformation by computed tomography in patients with leprosy. PLoS Negl Trop Dis 12(3):e0006341. https://doi.org/10.1371/journal.pntd.0006341

18. Caloss R, Atkins K, Stella JP (2007) Three-dimensional imaging for virtual assessment and treatment simulation in orthognathic surgery. Oral Maxillofac Surg Clin North Am 19(3):287–309. https://doi.org/10.1016/j.coms.2007.04.006

19. Swennen GR, Mollemans W, Schutyser F (2009) Three-dimensional treatment planning of orthognathic surgery in the era of virtual imaging. J Oral Maxillofac Surg 67(10):2080–2092. https://doi.org/10.1016/j.joms.2009.06.007

20. Wagner F, Dvorak G, Nemec S, Pietschmann P, Traxler H, Schicho K, Seemann R (2017) Morphometric analysis of sinus depth in the posterior maxilla and proposal of a novel classification. Sci Rep 7:45397. https://doi.org/10.1038/srep45397

21. Varga V, Raith S, Loberg C, Modabber A, Bartella AK, Holzle F, Fischer H, Steiner T (2017) Classification of the level of mandibular atrophy - a computer-assisted study based on 500 CT scans. J Craniomaxillofac Surg 45(12):2061–2067. https://doi.org/10.1016/j.jcms.2017.09.014

22. Raith S, Varga V, Steiner T, Hölzle F, Fischer H (2017) Computational geometry assessment for morphometric analysis of the mandible. Comput Methods Biomech Biomed Eng 20(1):27–34. https://doi.org/10.1080/10255842.2016.1196196

23. Horn B (1987) Closed-form solution of absolute orientation using unit quaternions. J Otical Soc Am 4:629–642

24. Park HS, Lee YJ, Jeong SH, Kwon TG (2008) Density of the alveolar and basal bones of the maxilla and the mandible. Am J Orthod Dentofac Orthop 133(1):30–37. https://doi.org/10.1016/j.ajodo.2006.01.044

25. Ali Hasan H, Khursheed Alam M, Yusof A, Matsuda S, Shoumura M, Osuga N (2016) Accuracy of three dimensional CT craniofacial measurements using mimics and Invesalius software programs. J Hard Tissue Biol 25(2):219–224. https://doi.org/10.2485/jhtb.25.219

26. Terry BC, Zarb GA (1991) Report on the 4th international congress on preprosthetic surgery, Palm Springs, USA, 18-20 April, 1991. Int J Oral Maxillofac Surg 20(5):314–316. https://doi.org/10.1016/s0901-5027(05)80168-7

27. Muller F, Naharro M, Carlsson GE (2007) What are the prevalence and incidence of tooth loss in the adult and elderly population in Europe? Clin Oral Implants Res 18(Suppl 3):2–14. https://doi.org/10.1111/j.1600-0501.2007.01459.x

28. Azarpazhooh A, Dao T, Ungar WJ, Chaudry F, Figueiredo R, Krahn M, Friedman S (2014) Clinical decision making for a tooth with apical periodontitis: the patients; preferred level of participation. J Endod 40(6):784–789. https://doi.org/10.1016/j.joen.2014.01.045

29. Turkyilmaz I, Company AM, Mcglumphy EA (2010) Should edentulous patients be constrained to removable complete dentures? The use of dental implants to improve the quality of life for edentulous patients. Gerodontology 27(1):3–10. https://doi.org/10.1111/j.1741-2358.2009.00294.x

30. Azarpazhooh A, Dao T, Figueiredo R, Krahn M, Friedman S (2013) A survey of patients' preferences for the treatment of teeth with apical periodontitis. J Endod 39(12):1534–1541. https://doi.org/10.1016/j.joen.2013.07.012

31. Schriber M, Bornstein MM, Suter VGA (2019) Is the pneumatisation of the maxillary sinus following tooth loss a reality? A retrospective analysis using cone beam computed tomography and a customised software program. Clin Oral Investig 23(3):1349–1358. https://doi.org/10.1007/s00784-018-2552-5

32. Cho SH, Kim TH, Kim KR, Lee JM, Lee DK, Kim JH, Im JJ, Park CJ, Hwang KG (2010) Factors for maxillary sinus volume and craniofacial anatomical features in adults with chronic rhinosinusitis. Arch Otolaryngol Head Neck Surg 136(6):610–615. https://doi.org/10.1001/archoto.2010.75

33. Sahlstrand-Johnson P, Jannert M, Strombeck A, Abul-Kasim K (2011) Computed tomography measurements of different dimensions of maxillary and frontal sinuses. BMC Med Imaging 11:8–7. https://doi.org/10.1186/1471-2342-11-8

34. Mohlhenrich SC, Heussen N, Peters F, Steiner T, Holzle F, Modabber A (2015) Is the maxillary sinus really suitable in sex determination? A three-dimensional analysis of maxillary sinus volume and surface depending on sex and dentition. J Craniofac Surg 26(8):e723–e726. https://doi.org/10.1097/SCS.0000000000002226